Crystal Structure of the Zinc-Dependent β-Lactamase from *Bacillus cereus* at 1.9 Å Resolution: Binuclear Active Site with Features of a Mononuclear Enzyme[†,‡]

Stella Maris Fabiane,[§] Maninder K. Sohi,[§] Tommy Wan,[§] David J. Payne,[∥] John H. Bateson,[⊥] Tim Mitchell,[⊥,#] and Brian J. Sutton*[,§]

The Randall Institute, King's College London, 26-29 Drury Lane, London WC2B 5RL, U.K., Anti-Infectives Research, SmithKline Beecham Pharmaceuticals, 1250 South Collegeville Road, P.O. Box 5089, Collegeville, Pennsylvania 19426-0989, and SmithKline Beecham Pharmaceuticals, New Frontiers Science Park (North), Harlow, Essex CM19 5AW, U.K.

Received March 4, 1998; Revised Manuscript Received June 23, 1998

ABSTRACT: The structure of the zinc-dependent β-lactamase II from *Bacillus cereus* has been determined at 1.9 Å resolution in a crystal form with two molecules in the asymmetric unit and 400 waters (space group $P3_121$; $R_{cryst} = 20.8\%$). The active site contains two zinc ions: Zn1 is tightly coordinated by His86, His88, and His149, while Zn2 is loosely coordinated by Asp90, Cys168, and His210. A water molecule (W1) lies between the two zinc ions but is significantly closer to Zn1 and at a distance of only 1.9 Å is effectively a hydroxide moiety and a potential, preactivated nucleophile. In fact, Asp90 bridges W1 to Zn2, and its location is thus distinct from that of the bridging water molecules in the binuclear zinc peptidases or other binuclear zinc hydrolases. Modeling of penicillin, cephalosporin, and carbapenem binding shows that all are readily accommodated within the shallow active site cleft of the enzyme, and the Zn1-bound hydroxide is ideally located for nucleophilic attack at the β-lactam carbonyl. This enzyme also functions with only one zinc ion present. The Zn1−Zn2 distances differ in the two independent molecules in the crystal (3.9 and 4.4 Å), yet the Zn1−W1 distances are both 1.9 Å, arguing against involvement of Zn2 in W1 activation. The role of Zn2 is unclear, but the *B. cereus* enzyme may be an evolutionary intermediate between the mono- and bizinc metallo-β-lactamases. The broad specificity of this enzyme, together with the increasing prevalence of zinc-dependent metallo-β-lactamases, poses a real clinical threat, and this structure provides a basis for understanding its mechanism and designing inhibitors.

The principal mechanism by which bacteria develop resistance to penicillins, cephalosporins, and other related β-lactam antibiotics involves the production of enzymes known as β-lactamases which inactivate these compounds (*1*). The β-lactamases cleave open the essential β-lactam ring, rendering the antibiotics incapable of binding to their target proteins, which are the enzymes involved in bacterial cell wall biosynthesis. Four classes of β-lactamase have been characterized on the basis of primary structure, three of which (A, C, and D) contain a catalytic serine residue in their active site. Crystal structures of a number of these active serine enzymes have been determined, and a mechanism-based inhibitor of these enzymes, clavulanic acid, has been developed (*2*). The fourth class of β-lactamase, class B, comprises metalloenzymes, all of which probably utilize Zn^{2+} as the natural cofactor, although activity with other divalent ions has been reported (*3*). One characteristic of the class B enzymes is their broad substrate profile, which includes not only the penicillins and cephalosporins but also the more recently introduced carbapenems. This, together with their increasing incidence among clinically important microorganisms, and the fact that inhibitors of the serine enzymes are ineffective against the metallo-β-lactamases, have led to a realization that the metallo-β-lactamases now pose a real threat to the future efficacy of existing antibiotics (*4*). Inhibitors of this class of β-lactamase are now urgently required.

The first and for a long time the only member of class B was the zinc-dependent enzyme from *Bacillus cereus* (*5*), a protein of 227 residues (*6, 7*), originally known as β-lactamase II since this organism produces another β-lactamase of class A (*8*). However, metallo-β-lactamases have since been reported and sequenced from *Bacteroides fragilis*, *Aeromonas hydrophila*, *Xanthomonas maltophilia*, and *Serratia marcescens* (*9* and references therein), as well as others for which sequences are not yet available (*4*). All those for which sequences are known appear to be related, if distantly, but it may be that other classes of metallo-β-lactamase do exist. The *B. cereus* enzyme was shown in early studies to bind two zinc ions, one with an affinity ≈1 μM (*3*) and the other ≈24 mM (*10*), although only one zinc ion was

[†] This work was supported by Grant G8817194 from the Medical Research Council, U.K.

[‡] The structure has been deposited in the Brookhaven Protein Data Bank, Brookhaven National Laboratories, Upton, Long Island, NY 11973-5000, under file names 1BC2 (coordinates) and R1BC2SF (structure factors).

* To whom correspondence should be addressed. E-mail: brian@helios.rai.kcl.ac.uk.

[§] King's College London.

[∥] SmithKline Beecham Pharmaceuticals, PA.

[⊥] SmithKline Beecham Pharmaceuticals, U.K.

[#] Current address: Oxford Molecular Ltd., The Medawar Centre, Oxford Science Park, Oxford OX4 4GA, U.K.

S0006-2960(98)00506-6 CCC: $15.00
Published on Web 08/20/1998

apparently required for activity (*3*). Substitution of the zinc ions by Co^{2+}, Cd^{2+}, Mn^{2+}, or Hg^{2+} led to much lower, but still significant levels of activity (*3*), and the first reported crystallization of the enzyme was in the presence of Cd^{2+} (*11*).

The structure of the zinc-containing β-lactamase from *B. cereus* has recently been solved at 2.5 Å resolution (*12*) in the same crystal form, space group *C*2, as that of the Cd^{2+} enzyme (*11*). One zinc ion was found at the active site. More recently, however, the structure of the homologous zinc-containing β-lactamase from *B. fragilis* was determined in two different space groups at 1.85 and 2.0 Å resolution (*13*, *14*), and in this enzyme *two* zinc ions were found in the active site. We report here the independent structure determination of the β-lactamase from *B. cereus* at 1.9 Å resolution in a new crystal form, $P3_121$, with two molecules in the asymmetric unit. Each of the two active sites contains two zinc ions. We therefore propose a mechanism of β-lactam hydrolysis for the *B. cereus* enzyme involving the two zinc ions, although it appears that the enzyme can function in the presence of either one or two zinc ions.

MATERIALS AND METHODS

Crystallization. Metallo-β-lactamase II from *B. cereus* 569/H (Public Health Laboratory Service, Porton Down, U.K.) was crystallized using the hanging drop vapor diffusion technique. Lyophilized protein as supplied was dissolved to a concentration of 2 mg/mL and 500 μM $ZnSO_4$ in 10 mM Tris-HCl buffer at pH 7.0 with 0.125% (w/v) sodium azide. The reservoir solution contained 500 μL of 10 mM Tris-HCl buffer, adjusted to pH 4.5 with HCl, and 0.125% (w/v) sodium azide, with 70%−75% (v/v) saturated ammonium sulfate. The hanging drops consisted of 3 μL of protein solution and 3 μL of reservoir solution diluted 2-fold with 100 mM Tris-HCl at pH 4.5 containing azide. The drops were kept at 18−20 °C, and large single crystals appeared within 1−2 weeks, by which time the pH of the drop had stabilized at 5.2 ± 0.1. The space group was found to be $P3_121$, and crystal density measurements (1.42 ± 0.01 g·cm^{-3}) and V_m ratio calculation (2.4 Å^3/Da) indicated two molecules in the asymmetric unit.

Data Collection and Processing. X-ray data to 2.5 Å resolution were collected using an RAXIS-IIC imaging plate detector mounted on a Rigaku RU200HB rotating anode (λ = 1.54 Å) and to 1.9 Å using a Mar 30 cm imaging plate area detector on station 9.6 at the Synchrotron Radiation Source, Daresbury Laboratory, U.K. (λ = 0.87 Å) at temperatures of 18 °C (capillary mounted) and −138 °C, respectively (flash frozen with 18% glycerol in mother liquor). The X-ray intensities were processed using DENZO (*15*) and the CCP4 (*16*) programs ROTAPREP, SORTMTZ, SCALA (*17*), AGROVATA, and TRUNCATE (*18*). The statistics for data collection and processing are presented in Table 1.

Structure Determination and Refinement. The structure was solved by multiple isomorphous replacement with data from two derivatives (Table 2) combined with solvent flipping and noncrystallographic symmetry averaging. The difference Patterson map at 3.5 Å for the Pt derivative, and difference Fourier maps, revealed four Pt binding sites that were refined with MLPHARE (*19*). These four sites provided the initial phasing power (Table 2) with an overall figure of merit of 0.37. The program SOLOMON (*20*) was then used to perform solvent flipping and automatic mask calculation. At this stage three α-helices and nine β-strands were identified for each molecule, and the program O (*21*) was used to create and edit a Cα skeleton. The noncrystallographic symmetry (NCS)[1] matrix was obtained by visual inspection and improved using IMP [part of the RAVE package (*22*, *23*)], with a correlation coefficient of 54.1% between the two molecules. Solvent flipping was performed again, combined with NCS averaging, and the correlation coefficient for the electron density inside the two NCS-related masks improved from 37.1% to 81.9%. A polyglycine model for the identifiable regions of secondary structure was refined with X-PLOR (*24*); 6% of the reflections were omitted and used for monitoring the progress of refinement [R_{free} test set (*25*)]. Phases calculated from the model were combined with the Pt-derived phases, and after solvent flipping and NCS averaging, a polyalanine model was built for the same regions as before and refined. The phases from this model were used to calculate a difference Fourier map with the uranyl derivative, and five sites were located. The Pt and U sites were refined with MLPHARE (combined figure of merit 0.47) and then further combined with phases from the polyalanine model for another round of solvent flipping and NCS averaging. At this stage, data collected from an EDTA-soaked crystal were used to calculate a difference Fourier map in which one zinc atom could be located per molecule; this enabled residues 153−227 to be traced, retaining the remainder as polyalanine. This new model was refined and used for a further round of solvent flipping and NCS averaging, after which the whole region from residue 40 to residue 227 could be traced. At this point, data to 2.65 Å

Table 1: Native Data Collection and Processing Statistics

space group	$P3_121$	$P3_121$
unit cell		
$a = b$ (Å)	68.1	67.6
c (Å)	180.9	178.4
resolution limit (Å)	2.5	1.9
no. of unique reflections	16104	37064
average redundancy[a]	4.1	2.3
completeness overall[b] (%) [outer shell, 1.95−1.9 Å]		99.4 [99.7]
R_{sym}[c] (%) [outer shell, 1.95−1.9 Å]	4.5	5.4 [28.9]

[a] Redundancy = (number of measurements)/(number of independent reflections). [b] Completeness = 100(number of independent reflections measured)/(theoretical maximum number of reflections). [c] $R_{sym} = \sum_h\sum_i|I_i(h) - \langle I(h)\rangle|/\sum_h\sum_i I_i(h)$, where $I(h)$ is the measured intensity and $\langle I(h)\rangle$ is the mean of i measurements.

Table 2: Statistics for the Isomorphous Derivative Data Sets

derivative	K_2PtCl_4	$UO_2(NO_3)_2$	EDTA
soak conditions	4 mM, 3 days, pH 6.0	2.5 mM, 3 days, pH 4.5	0.25 mM, 6 days, pH 4.5
resolution limit (Å)	3.3	3.5	3.5
completeness (%)	99.9	99.9	93.6
R_{sym}[a] (%)	5.8	8.3	8.1
R_{diff}[b] (%)	23.8	18.0	27.9
phasing power[c]	1.61	1.00	
no. of sites	4	5	

[a] $R_{sym} = \sum_h\sum_i|I_i(h) - \langle I(h)\rangle|/\sum_h\sum_i I_i(h)$. [b] $R_{diff} = \sum_h|F_{PH} - F_P|/\sum_h|F_P|$. [c] Phasing power = $\langle F_H\rangle/\langle E\rangle$, where E is the lack-of-closure error.

[1] Abbreviations: NCS, noncrystallographic symmetry; rms, root mean square; F_o and F_c, observed and calculated structure factors.

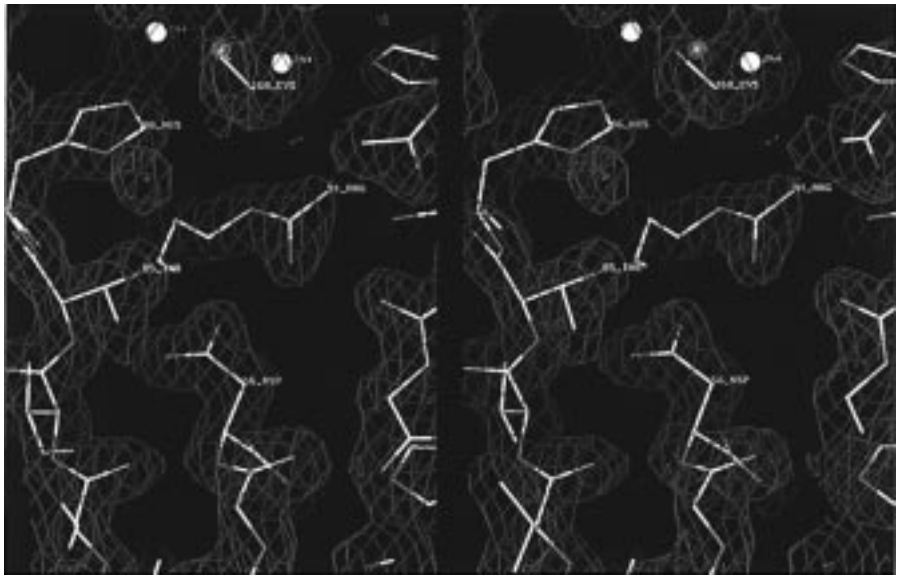

FIGURE 1: Stereoview of the environment of Asp56, the only residue in a forbidden region of the Ramachandran plot. SIGMAA-weighted (*29*) $2F_o - F_c$ electron density map (all atoms included) at 1.9 Å resolution is contoured at 1.2σ. Four hydrogen bonds stabilize the strained backbone conformation of Asp56, one of which links Asp56 to Arg91, immediately beneath the catalytic zinc ions. The image was drawn using the program QUANTA (*27*).

were included, and after the subsequent refinement cycle residues 7−32 could be traced.

The structure was refined using X-PLOR and manual model building performed with O. The first rounds of refinement used strict NCS, but subsequent refinement used restrained NCS, gradually decreasing the weights to 40 kcal/mol for protein atoms and 20 kcal/mol for nonbonded atoms (zinc, sulfate, and water molecules). The upper resolution limit for reflections throughout refinement was 8 Å. After the inclusion of data to 2.5 Å and further refinement, the model for each molecule contained 215 of the 227 residues, 1 zinc ion, 2 sulfate ions, and 19 water molecules, plus a further 62 water molecules not related by NCS. No electron density was visible for residues 1−6 or 33−37. The N-terminus of the enzyme was known to be "ragged" (*26*), but mass spectroscopic analysis of crystals revealed that selective crystallization of a form lacking residues 1−4 had occurred; thus only the two N-terminal residues 5 and 6 are in fact disordered. The disordered loop 33−37 will be discussed below. At this stage R_{free} was 26.8% and R_{cryst} (calculated on the working set of reflections) was 19.2%. The data set to 1.9 Å was then used, and after five rounds of refinement the NCS restraints were removed entirely. Further water molecules (total 400) were identified with QUANTA (*27*), as well as a second zinc ion, interpreted earlier at 2.5 Å resolution as a sulfate ion. The final R_{free} was 27.9%, and R_{cryst} (calculated on all reflections after the final round of refinement) was 20.8%. The van der Waals radius used for the zinc ion was 1.15 Å. Larger radii were tested but led to W1 moving out of electron density; lower values did not affect the refined atomic position. No constraints were placed on any atoms, except for the NCS constraints in the early stages of refinement. For the final five rounds of refinement the electrostatic energy term was switched off.

The geometry of the model is good as assessed by PROCHECK (*28*), although one residue, Asp56, lies in a forbidden region of the Ramachandran plot ($\phi = 74.5°$, $\varphi = 150.8°$ in molecule A, $\phi = 75.6°$, $\varphi = 150.0°$ in molecule B). This residue lies immediately adjacent to the active site, and its electron density may be seen in Figure 1 (which also illustrates the quality of the map at this resolution). The statistics for the final model are given in Table 3. The mean coordinate error, as estimated by the SIGMAA method (*29*), is 0.3 Å.

Table 3: Refinement Statistics

resolution range (Å)	8.0−1.9
no. of reflections	37064
no. of protein atoms per asymmetric unit	3346
no. of water molecules per asymmetric unit	400
no. of sulfate ions per asymmetric unit	2
no. of zinc atoms per asymmetric unit	4
R_{cryst}[a] (%)	20.8
R_{free}[b] (%)	27.9
average *B* factor for protein atoms (Å^2)	29.81
average *B* factor for water molecules (Å^2)	43.98
rms deviation, bond lengths (Å)	0.007
rms deviation, bond angles (deg)	1.350
rms deviation, dihedral angles (deg)	24.093
rms deviation, improper torsion angles (deg)	1.238
rms deviation between the NCS-related molecules (Å, all atoms)	0.911

[a] $R_{cryst} = \sum_h||F(h)_o| - |F(h)_c||/\sum_h|F(h)_o|$ for all reflections [b] $R_{free} = \sum_h||F(h)_o| - |F(h)_c||/\sum_h|F(h)_o|$ for a randomly selected 6% set of reflections not used in refinement.

RESULTS AND DISCUSSION

Overall Architecture. The structure consists of a sandwich of two twisted β-sheets, each flanked on their outer face by two α-helices, with a fifth helix bridging the two sheets (Figure 2). This fold is exactly as reported by Carfi et al. (*12*) (rms deviation between backbone atoms = 0.46 Å) and similar also to that of the *B. fragilis* enzyme (*13*, *14*) (rms deviation between backbone atoms = 1.18 Å). The active site, identified in Figure 2 by the two zinc ions shown in green, lies at one edge of the β-sheet sandwich, and the ligand residues belong to segments of polypeptide chain which form extended loops connecting the secondary structural elements.

FIGURE 2: Ribbon representation of the enzyme showing the two β-sheets flanked by α-helices; the latter, together with the N- and C-termini, are labeled. The active site residues are shown, colored according to secondary structure (α-helix, yellow; β-strand, purple; random coil, white) with the two zinc ions (green). The image was drawn using the program SETOR (*48*).

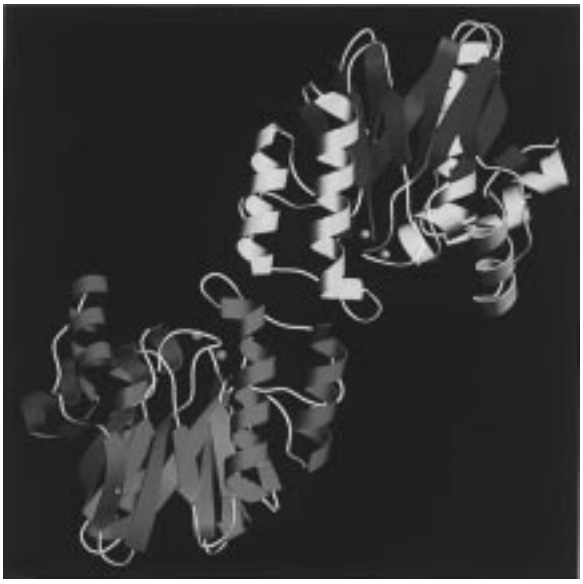

FIGURE 3: Noncrystallographic symmetry interaction. The two C-terminal α-helices (α4 and α5) of each molecule pack "head to tail", forming continuous intermolecular helical structures. The 2-fold NCS axis passes through the center of the image, perpendicular to the plane of the paper. The image was drawn using SETOR (*48*).

There is a degree of similarity between this fold and that of the N-terminal nucleophile (Ntn) aminohydrolases (*30*). While the architecture of the Ntn hydrolase family, which tantalizingly includes the enzyme penicillin acylase (*31*), consists of a sandwich of two five-stranded β-sheets flanked on each side by two α-helices, the connectivities between the strands and helices are quite different from that in the metallo-β-lactamase. Any similarity therefore would appear to be merely an example of convergence to a stable arrangement of secondary structural elements.

Noncrystallographic Symmetry. The NCS axis is an almost exact 2-fold (179.5° rotation and no translation) as shown in Figure 3, and intermolecular contact occurs between the two C-terminal α-helices (α4 and α5). These helices pack head to tail, and intermolecular hydrogen bonds between the peptide units form, in effect, a continuous helical structure spanning the two molecules. The active sites of the two enzyme molecules are brought within 24 Å of each other in the crystal through this interaction (Figure 3), but there is no evidence for dimerization of the enzyme in solution.

The Active Site. The active site contains two zinc ions, liganded by residues that are almost entirely conserved in all the known metallo-β-lactamase sequences. Zn1 [which corresponds to the single zinc ion identified by Carfi et al. at 2.5 Å resolution (*12*)] is liganded by the three histidine residues, 86, 88, and His149, and a water molecule (W1) in a tetrahedral arrangement. Both His86 and 149 use the Nϵ2 atom of the imidazole ring, as is commonly observed, whereas His88 interacts via the Nδ1 atom. The electron density corresponding to this region is shown in Figure 4. The second zinc ion is liganded by Asp90, Cys168, and the Nϵ2 atom of His210, together with two water molecules, W1 and W2, providing 5-fold coordination in a distorted trigonal bipyramidal arrangement (Figure 4). W1, which might appear to bridge the two zinc ions, lies very much closer to Zn1 than to Zn2 (Figure 4 and Table 4), and the two zinc ions are in fact bridged by W1 and Asp90 in series. In this respect the active site differs strikingly from those of the binuclear zinc peptidases (*32*−*35*) and other hydrolases (*36*−*39*), in which a water molecule and a protein side chain (carboxylate) each independently bridge the two zinc ions in parallel.

While the structures of the two independently refined active sites are essentially identical, two interatomic distances differ significantly (Table 4). These are the Zn1−Zn2 and the Zn2−W1 distances, which differ by 0.5 and 0.6 Å, respectively, substantially greater than the mean coordinate error of 0.3 Å (see Materials and Methods) and in contrast to all of the other Zn−ligand distances, which differ by less than 0.2 Å between the two molecules. In Figure 5, the two active site structures are superimposed, by best-fitting Zn1 and its ligands. It is clear that the difference between the two sites is a shift of Zn2, together with His210 and W2, away from Zn1. This contrast between virtually identical Zn1 sites, and conformationally variable Zn2 sites with "looser" arrangement of ligands, is consistent with their different affinities for zinc and is also reflected in the temperature factors (Zn1, 31 and 32 Å^2; Zn2, 53 and 62 Å^2), refined assuming full occupancy. Another difference that can be seen in Figure 5 is the conformation of Lys171, a residue conserved in all but the *X. maltophilia* enzyme, which forms a weak hydrogen bond to W2 (Table 4).

W1 is very closely associated with Zn1 (*B* factors, 26 and 26 Å^2, cf. 41 and 32 Å^2 for W2), and significantly, the movement of Zn2 away from Zn1 by 0.5 Å in molecule B relative to molecule A has no effect upon the Zn1−W1 distance, which remains at 1.9 Å in both molecules (Table 4). This is as short as the Zn−O bond lengths in tetrahedrally coordinated hydroxy salts (2.0 Å) or zinc oxide (*40*) (1.95 Å) and must be a hydroxide moiety. It also forms a hydrogen bond to Asp90 (2.8 Å in both molecules, Table 4), which in turn forms a hydrogen bond to Zn2 (2.8 and 2.9 Å).

The two zinc ions lie in a shallow cleft, both readily accessible to solvent. One side of this cleft is formed by

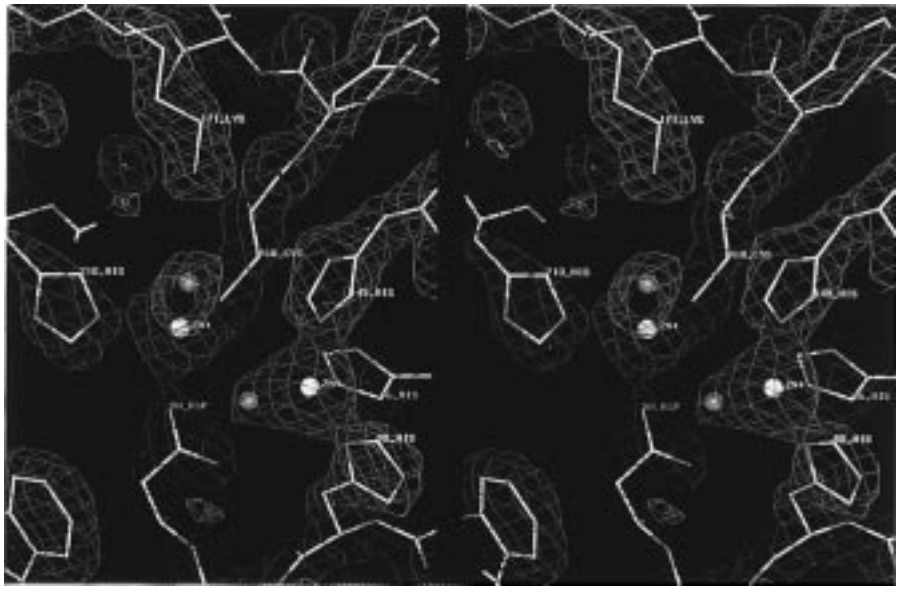

FIGURE 4: Stereoview of the active site. SIGMAA-weighted (*29*) $2F_o - F_c$ map (all atoms included) is contoured at 1.2σ (molecule B). Zn1 is tetrahedrally coordinated by His86, His88, His149, and the water molecule W1 (red). Zn2 is coordinated by Asp90, Cys168, His210, W2, and W1. Lys171 points toward W2. Other water molecules are represented by red crosses. The image was drawn using QUANTA (*27*).

Table 4: Interatomic Distances (Å) in the Active Sites of the Two Molecules in the Asymmetric Unit

atoms involved	A	B
Zn1···Nϵ2 (His86)	2.27	2.24
Zn1···Nδ1 (His88)	1.95	2.16
Zn1···Nϵ2 (His149)	2.00	2.11
Zn1···W1	1.90	1.90
Zn1···Zn2	3.85	4.36
Zn2···W1	2.48	3.06
Zn2···Oδ2 (Asp90)	2.75	2.90
Zn2···Sγ (Cys168)	1.91	1.98
Zn2···Nϵ2 (His210)	2.59	2.45
Zn2···W2	2.55	2.69
W1···Oδ1 (Asp90)	2.79	2.84
W2···Nζ (Lys171)	4.01	3.33

residues Lys176 to Asp183, of which Gly179 and Asn180 are conserved in all known metallo-β-lactamase sequences. Their significance becomes clear when β-lactams are docked into the active site (see below). The two ends of the cleft are apparently open, although the disordered loop region, residues 33−37, lies at one end. No electron density is visible at all for these five residues; the corresponding loop in the *B. fragilis* enzyme is one residue longer, and two residues similarly lack electron density (*13*). As suggested by Concha et al., this loop may interact with substrate (*13*) or even close over the active site. Chemical modification of one of the disordered loop residues in the *B. cereus* enzyme, Glu37, was reported to block activity (*41*), consistent with its proximity to the active site, but mutation of this residue to Gln (*42*) later showed that it was not essential for activity.

Finally, a buried salt bridge, Arg91−Asp56, lies immediately below the zinc ions in the "floor" of the active site (Figure 1). An extensive hydrogen-bonding network links Arg91 to Asp90 and Gly209; the adjacent residue His210, and Asp90, are Zn2 ligands, and thus Arg91 is involved in shaping the Zn2 site as well as contributing to the electrostatic environment of the active site.

Modeling of Substrate Binding. The shallow, accessible active site cleft allows β-lactam substrates with very different side chains attached to the β-lactam nucleus to be "docked" in a similar way, consistent with the broad activity profile of this enzyme. Substrates were located such that the common carboxylate group of the five- (or six-) membered ring pointed toward the conserved Lys171 and the β-lactam carbonyl pointed between Zn1 and the Nδ of conserved Asn180. Panels a and b of Figure 6 show the proposed binding of benzylpenicillin and meropenem. In this mode of binding, which is very similar to that proposed by Concha et al. for the *B. fragilis* enzyme (*13*), W1 lies immediately beneath the β-lactam carbonyl carbon, ideally located for nucleophilic attack (Figure 6). W2, however, is displaced by the substrate's carboxylate group, which may interact with, and maintain pentacoordination at, Zn2. In this respect, our model differs from that of Concha et al. (*13*), in which W2 (their "apical" water molecule), is not displaced; indeed, these authors propose that, with a slight shift of the substrate, W2 could be the nucleophile. Carfi et al. (*14*) propose a model for substrate binding to the *B. fragilis* enzyme in which W2 is displaced, but the carboxylate interacts with Zn2 and not Lys171. In the same authors' model for substrate binding to the monozinc *B. cereus* enzyme, the carboxylate interacts with His210 (*12*).

Neither of these models of substrate binding to *B. fragilis*, nor that of Carfi et al. to the *B. cereus* enzyme, explains the absolute conservation of Gly179 in all known metallo-β-lactamase sequences, but in the model proposed here it is clear that any side chain at this position would prevent substrate binding (Figure 6). Furthermore, the conformational variability of the side chain of Lys171, as seen in the two molecules in the asymmetric unit, may also be important in allowing the interaction with the conserved carboxylate group to be maintained despite the latter's slightly different orientation with respect to the β-lactam ring in the different substrates.

Catalytic Mechanism. We propose that water molecule W1, so closely associated with Zn1 that it is best described as a hydroxide, is the preactivated nucleophile that attacks the β-lactam carbonyl carbon atom. In the Michaelis

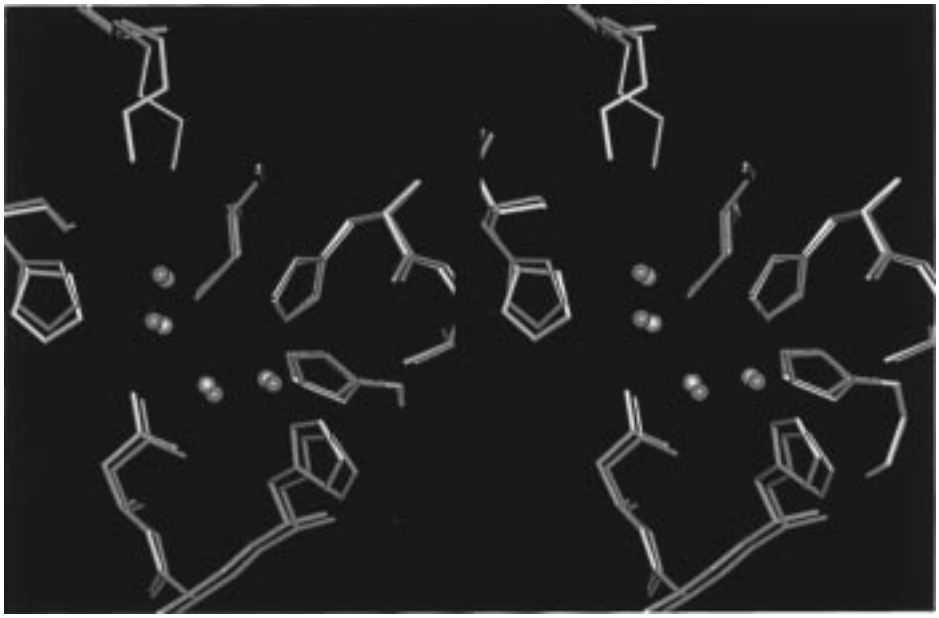

FIGURE 5: Stereoview of the superimposed active sites in the two molecules (A, green; B, magenta). The structures were best-fitted on Zn1 and its ligands; differences at the Zn2 site are apparent. The image was drawn using QUANTA (*27*).

complex (shown schematically in Figure 7), the β-lactam carbonyl oxygen interacts with Zn1, which expands its coordination number to 5, and serves to polarize the carbonyl bond enhancing its susceptibility to nucleophilic attack. At Zn2, one oxygen atom of the substrate's conserved carboxylate moiety replaces W2, while the other interacts with Lys171. As hydroxide W1 attacks the β-lactam carbonyl bond, the lone pair of the β-lactam nitrogen atom may interact with Zn2, maintaining its pentacoordination. As the transition state develops, with tetrahedral coordination at the β-lactam carbonyl carbon atom, Asn180 NδH and Zn1 can stabilize the oxyanion. Asp90, initially hydrogen bonded to the zinc-bound hydroxide, is ideally located to accept the proton from the hydroxide and, as β-lactam bond cleavage occurs, protonate the nitrogen atom. Mutagenesis has demonstrated that this residue indeed performs a critical role in the *B. cereus* enzyme (*43*).

Deprotonation of the hydroxide by Asp90 implies the formation of a dianion, and mechanistic studies by Bounaga et al. indicate that a dianionic species is indeed formed, since there is an inverse *second*-order dependence of reactivity of the *B. cereus* enzyme upon hydrogen ion concentration at low pH (*44*). This is in contrast to the mechanism proposed by Concha et al. (*13*), which does not invoke a dianion; furthermore, Concha et al. suggest that W2 donates the proton to the β-lactam nitrogen (or may even be the nucleophile). These authors do draw attention to the differences between the pH dependence of k_{cat} for the *B. fragilis* (*13*) and *B. cereus* enzymes at low pH (*45*), which may reflect real mechanistic differences.

The location of W1 is quite distinct from that of the water molecules that bridge the two zinc ions in the binuclear zinc peptidases (*32*−*35*) or in other binuclear zinc hydrolases such as nuclease P1 (*36*), phospholipase C (*37*), or phosphotriesterase (*38*). In all of these structures the bridging water molecule, the presumed nucleophile, is symmetrically placed between the two zinc ions (2.0−2.3 Å from each). The longer W1−Zn2 distances in the *B. cereus* enzyme (2.5 and 3.1 Å, Table 4) argue against a role for Zn2 in activation of the water molecule. In fact, the location and role of Asp90 resemble the mononuclear zinc peptidases typified by carboxypeptidase A and thermolysin (*46*), and the mechanism of the *B. cereus* enzyme thus appears to exhibit features of both the mono- and binuclear zinc enzymes.

Mechanistic Duality of the B. cereus Metallo-β-lactamase. It is known that the *B. cereus* enzyme displays significant activity with only a 1:1 molar ratio of Zn^{2+} to enzyme (*3*), which, given the very different affinities of the two sites, would lead to occupancy only at Zn1. [We believe that the existence of only one zinc ion in the structure of Carfi et al. (*12*) is a result of the molar ratio of Zn^{2+} to enzyme of 0.3:1, compared with 6:1 in the present study.] In the absence of Zn2, the hydroxide W1 is expected to occupy the same location as seen in the two-zinc structure, since we observe that movement of Zn2 away from W1 by 0.6 Å in molecule B relative to molecule A (Figure 5 and Table 4) does not affect W1. Asp90 would still be able to deprotonate W1 and might be expected to act as a stronger conjugate base in the absence of Zn2.

What therefore is the role of Zn2? It may interact with substrate as described above or serve to orient Asp90. Certainly the *B. fragilis* enzyme, with two zinc sites of comparable affinity ($\approx$1 μM), will always contain two zinc ions (*13*). They are closer together (3.5 Å) than in the *B. cereus* enzyme (3.9 and 4.4 Å, Table 4), and the water molecule/hydroxide ion is almost symmetrically located between them, as in other binuclear zinc hydrolases (*13*). Functionally, while the substrate profiles of the two enzymes are similarly broad, the *B. fragilis* enzyme generally displays a higher catalytic efficiency [K_ms are typically 10−100-fold lower for the *B. fragilis* enzyme (*47*)]. Structurally, the Zn2 site in the *B. cereus* enzyme has a "loose" arrangement of ligands compared with the *B. fragilis* enzyme (e.g., His210 Nϵ2−Zn2, 2.5/2.6 and 2.1/2.2 Å, respectively), and Arg91, lying just below Zn2 in the former (Arg91 NH2−Zn2, 4 Å), will lower the affinity for Zn^{2+} at this site. In the *B. fragilis* enzyme this residue is replaced by cysteine. Both functionally and structurally therefore, the *B. cereus* enzyme appears

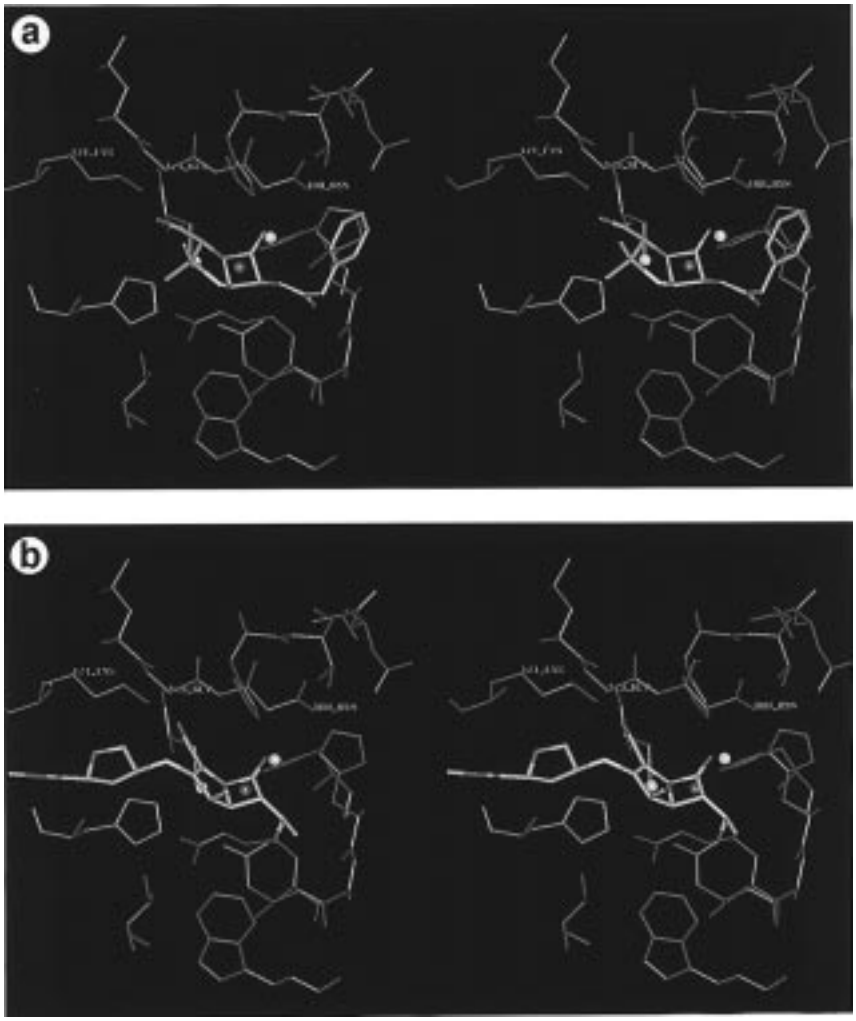

FIGURE 6: Stereoviews of the modeling of (a) benzylpenicillin, and (b) meropenem. Features common to the docked structures are the β-lactam carbonyl oxygen pointing between Zn1 and Nδ of Asn180, the substrate's carboxylate group pointing toward Lys171, and the displacement of W2. W1 is ideally placed to attack the β-lactam ring. Conservation of Gly179 is clearly required to allow substrate binding. Val39 (bottom left), at the C-terminal side of the disordered loop, is within 4.5 Å of the substrate, indicating the proximity of this flexible loop. The image was drawn using QUANTA (*27*).

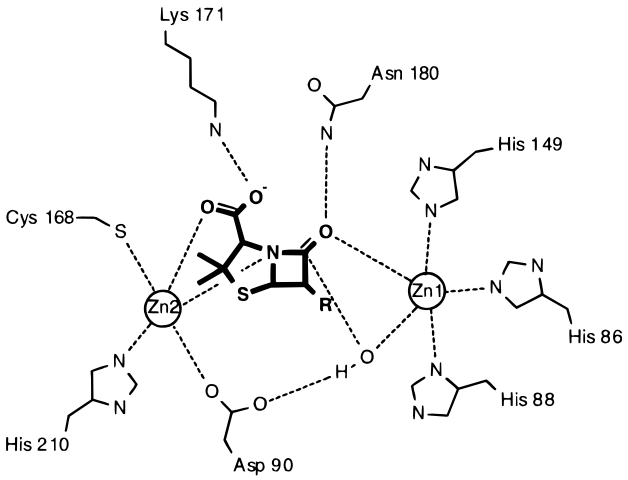

FIGURE 7: Schematic diagram of the proposed Michaelis complex for a penicillin bound to the enzyme. The hydroxide (W1) is activated by Zn1 for nucleophilic attack at the carbonyl carbon; the substrate's carboxylate group displaces W2 and interacts with Lys171 and Zn2.

to be the more "primitive" and may be an evolutionary intermediate between mononuclear β-lactamases and binuclear enzymes with two high-affinity sites.

The *B. cereus* enzyme thus displays a remarkable adaptability, able to function with either one or two zinc ions, or indeed other metal ions, and capable of hydrolyzing virtually all known β-lactam antibiotics. It is this latter capability which now poses such a serious clinical threat, and the need to design inhibitors of these enzymes is most urgent. Knowledge of this structure will, we hope, facilitate the process.

ACKNOWLEDGMENT

We thank Dr. Miroslav Papiz and others at the Daresbury Laboratory SRS for their contributions, David Tolson for mass spectroscopic analysis of the crystals, and Kate Kirwan and Mark Simon for production of the figures. We also acknowledge the contribution to this field of the late Dr. Stephen Waley, who first encouraged X-ray analysis of this enzyme.

REFERENCES

1. Frère, J.-M. (1995) *Mol. Microbiol. 16*, 385−395.
2. Chen, C. C. H., and Herzberg, O. (1992) *J. Mol. Biol. 224*, 1103−1113.
3. Davies, R. B., and Abraham, E. P. (1974) *Biochem. J. 143*, 129−135.

4. Payne, D. J. (1993) *J. Med. Microbiol. 39*, 93−99.
5. Sabath, L. D., and Abraham, E. P. (1966) *Biochem. J. 98*, 11c−13c.
6. Ambler, R. P., Daniel, M., Fleming, J., Hermoso, J. M., Pang, C., and Waley, S. G. (1985) *FEBS Lett. 189*, 207−211.
7. Hussain, M., Carlino, A., Madonna, M. J., and Lampen, J. O. (1985) *J. Bacteriol. 164*, 223−229.
8. Kuwabara, S., and Abraham, E. P. (1967) *Biochem. J. 103*, 27c−30c.
9. Rossollini, G. M., Walsh, T., and Amicosante, G. (1996) *Microb. Drug Resist. 2*, 245−252.
10. Baldwin, G. S., Galdes, A., Hill, H. A. O., Smith, B. E., Waley, S. G., and Abraham, E. P. (1978) *Biochem. J. 175*, 441−447.
11. Sutton, B. J., Artymiuk, P. J., Cordero-Borboa, A. E., Little, C., Phillips, D. C., and Waley, S. G. (1987) *Biochem. J. 248*, 181−188.
12. Carfi, A., Pares, S., Duée, E., Galleni, M., Duez, C., Frère, J.-M., and Dideberg, O. (1995) *EMBO J. 14*, 4914−4921.
13. Concha, N. O., Rasmussen, B. A., Bush, K., and Herzberg, O. (1996) *Structure 4*, 823−836.
14. Carfi, A., Duée, E., Paul-Soto, R., Galleni, N., Frère, J.-M., and Dideberg, O. (1998) *Acta Crystallogr. D54*, 47−57.
15. Otwinowski, Z. (1993) *Data Collection and Processing* (Sawyer, L., Isaacs, N., and Bailey, S., Eds.) pp 56−62, SERC, Daresbury Laboratory, Warrington, U.K.
16. CCP4, Collaborative Computational Project, Number 4 (1994) *Acta Crystallogr. D50*, 760−763.
17. Evans, P. R. (1993) *Data Collection and Processing* (Sawyer, L., Isaacs, N., and Bailey, S., Eds.) pp 114−122, SERC, Daresbury Laboratory, Warrington, U.K.
18. French, S., and Wilson, K. (1978) *Acta Crystallogr. A34*, 517−525.
19. Otwinowski, Z. (1991) *Isomorphous Replacement and Anomalous Scattering* (Wolf, W., Evans, P. R., and Leslie, A. G. W., Eds.) pp 80−86, SERC, Daresbury Laboratory, Warrington, U.K.
20. Abrahams, J. P., and Leslie, A. G. W. (1996) *Acta Crystallogr. D52*, 30−42.
21. Jones, T. A., Zou, J. Y., Cowan, S. W., and Kjelgaard, M. (1991) *Acta Crystallogr. A47*, 110−119.
22. Jones, T. A. (1992) *Molecular Replacement* (Dodson, E. J., Glover, S., and Wolf, W., Eds.) pp 92−105, SERC, Daresbury Laboratory, Warrington, U.K.
23. Kleywegt, G. J., and Jones, T. A. (1994) *From First Map to Final Model* (Bailey, S., Hubbard, R., and Waller, D., Eds.) pp 59−66, SERC, Daresbury Laboratory, Warrington, U.K.
24. Brünger, A. T. (1992) *X-PLOR Version 3.2: A system for X-ray crystallography and NMR*, Yale University Press, New Haven, CT.
25. Brünger, A. T. (1992) *Nature 355*, 472−475.
26. Payne, D. J., Skett, P. W., Aplin, R. T., Robinson, C. V., and Knowles, D. J. C. (1994) *Biol. Mass Spectrom. 23*, 159−164.
27. Molecular Simulations Inc. (1996) *QUANTA96*, San Diego, CA.
28. Laskowski, R. A., MacArthur, M. W., Moss D. S., and Thornton J. M. (1993) *J. App. Crystallogr. 26*, 283.
29. Read, R. J. (1986) *Acta Crystallogr. A42*, 140−149.
30. Artymiuk, P. J. (1995) *Nat. Struct. Biol. 2*, 1035−1037.
31. Duggleby, H. J., Tolley, S. P., Hill, C. P., Dodson, E. J., Dodson, G., and Moody, P. C. E. (1995) *Nature 373*, 264−268.
32. Sträter, N., and Lipscomb, W. N. (1995) *Biochemistry 34*, 14792−14800.
33. Chevrier, B., Schalk, C., D'Orchymont, H., Rondeau, J. M., Moras, D., and Tarnus, C. (1994) *Structure 2*, 283−291.
34. Greenblatt, H. M., Almog, O., Maras, B., Spungin-Bialik, A., Barra, D., Blumberg, S., and Shoham, G. (1997) *J. Mol. Biol. 265*, 620−636.
35. Rowsell, S., Pauptit, R. A., Tucker, A. D., Melton, R. G., Blow, D. M., and Brick, P. (1997) *Structure 5*, 337−347.
36. Volbeda, A., Lahm, A., Sakiyama, F., and Suck, D. (1991) *EMBO J. 10*, 1607−1618.
37. Hough, E., Hansen, L. K., Birknes, B., Jynge, K., Hansen, S., Hordvik, A., Little, C., Dodson, E., and Derewenda, Z. (1989) *Nature 338*, 357−360.
38. Vanhooke, J. L., Benning, M. M., Raushel, F. M., and Holden, H. M. (1996) *Biochemistry 35*, 6020−6025.
39. Wilcox, D. E. (1996) *Chem. Rev. 96*, 2435−2458.
40. Wells, A. F. (1967) *Structural Inorganic Chemistry*, 3rd ed., pp 395 ff and 506 ff, Oxford University Press, Oxford, U.K.
41. Little, C., Emanuel, E. L., Gagnon, J., and Waley, S. G. (1986) *Biochem. J. 233*, 465−469.
42. Lim, H. M., and Pène, J. J. (1989) *J. Biol. Chem. 264*, 11682−11687.
43. Lim, H. M., Iyer, R. K., and Pène, J. J. (1991) *Biochem J. 276*, 401−404.
44. Bounaga, S., Laws, A. P., Galleni, M., and Page, M. I. (1998) *Biochem. J. 331*, 703−711.
45. Bicknell, R., Knott-Hunziker, V., and Waley, S. G. (1983) *Biochem. J. 213*, 61−66.
46. Lipscomb, W. N., and Sträter, N. (1996) *Chem. Rev. 96*, 2375−2433.
47. Felici, A., Amicosante, G., Oratore, A., Strom, R., Ledent, P., Joris, B., Fanuel, L., and Frère, J.-M. (1993) *Biochem. J. 291*, 151−155.
48. Evans, S. V. (1993) *J. Mol. Graphics 11*, 134−138.

BI980506I